

# **Staggered grids for 3D pseudospectral modelling in anisotropic elastic media**

Richard A. Bale

## **ABSTRACT**

Pseudospectral modeling is an alternative to finite-difference that is based on Fourier spatial operators. It can be applied in 3D to anisotropic elastic media. The nature of non-causal artifacts, which arise during pseudospectral modelling, is reviewed. They are a result of Nyquist discontinuities in the periodic wavenumber spectrum. The well-known solution, using staggered grids, can be made exact for isotropy or for anisotropy with at least orthorhombic symmetry, but cannot be done exactly for general anisotropy. Further interpolation or shifting is required. The stress-strain relationship can be factorized into an orthorhombic type term, where the staggering is exact, and a residual term where the shifting operations are applied as diagonal matrices. Examples illustrate the benefit of using this scheme over the standard (non-staggered) grid approach.

## **INTRODUCTION**

The pseudospectral method (Kosloff and Baysal, 1982) is a grid based modelling method similar to finite difference, with one key difference. Instead of using difference operators, Fourier transforms are used to apply the spatial derivatives. It can be viewed as a limiting case of higher order finite difference, when the operator size equals the grid dimension. The main advantage, for seismic modelling, is that it requires considerably fewer grid points per wavelength, to attain any desired accuracy. According to Fornberg (1987), a fourth order finite difference code needs 4 times as many grid points per wavelength as the pseudospectral approach, along each spatial dimension. Hence, the pseudospectral method is particularly attractive for modelling in 3D.

However, the pseudospectral method is not without its own difficulties. These include unbalanced numerical dispersion, due to the use of a difference approximation in the time marching, and wrap-around artifacts, due to the periodicity implied by using the Fourier domain. The first of these can be addressed by the use of higher order operators (Dablain, 1986). The second requires the use of absorbing boundaries (Cerjan et al., 1985), or perfectly matched layers (Collino and Tsogka, 2001).

Another difficulty, and the subject of this paper, is the generation of non-causal ringing artifacts, particularly in the presence of large abrupt changes in the medium. It is well established (Özdenvar and McMechan, 1996; Corrêa et al., 2002) that modelling on a staggered grid mitigates these effects. Staggered grids are also used in finite difference modelling to ensure centred derivatives. The extension to general anisotropy gives rise to complications with the staggering schemes for both finite difference and pseudospectral methods (Igel et al., 1995; Carcione et al., 2002). In the first section of this paper, I describe a staggering scheme for 3D pseudospectral modelling in fully anisotropic media. This is based upon decomposing the anisotropy into orthorhombic and non-orthorhombic stiffnesses. In the second part, I show some simple examples to illustrate the effect of staggering the grid for different anisotropies.

## THEORY

The modelling of wave propagation in elastic, anisotropic, heterogeneous media is based upon the following equation of motion:

$$\rho \ddot{u}_j = \sigma_{jl,l} + f_j \quad (1)$$

where  $\rho$  is density,  $u_j$  is the component of displacement in the  $j^{\text{th}}$  direction, and  $f_j$  is the body force which in this case is taken to be the source term.

Above, and throughout this paper, I use the convention that “ $l$ ” denotes partial differentiation with respect to  $x_l$ , the  $l^{\text{th}}$  spatial coordinate, and also the Einstein summation convention whereby twice-repeated indices indicate an implied summation. Suffices repeated more than twice imply that the summation convention is suspended. All suffices take the values 1,2 and 3, and to clarify I use  $x,y$  and  $z$  when appropriate. Also  $\ddot{u}$  indicates the second time derivative of  $u$ . The stress-strain relationship (generalized Hooke’s law) between the stress  $\sigma_{jl}$ , and the strain  $e_{mn}$ , is given by:

$$\sigma_{jl} = c_{jlmn} e_{mn} \quad (2)$$

where  $c_{jlmn}$  is the 4<sup>th</sup> rank stiffness tensor. In turn the strain tensor is given by:

$$e_{mn} = 1/2(u_{m,n} + u_{n,m}) \quad (3)$$

An alternative representation of the stiffness tensor uses the Voigt notation to replace the 4<sup>th</sup> rank tensor  $c_{jlmn}$  by a symmetric 6x6 matrix  $\mathbf{C}$  as follows:

$$\mathbf{C} \equiv \begin{bmatrix} c_{1111} & c_{1122} & c_{1133} & c_{1123} & c_{1113} & c_{1112} \\ & c_{2222} & c_{2233} & c_{2223} & c_{2213} & c_{2212} \\ & & c_{3333} & c_{3323} & c_{3313} & c_{3312} \\ & & & c_{2323} & c_{2313} & c_{2312} \\ & & & & c_{1313} & c_{1312} \\ & & & & & c_{1212} \end{bmatrix} \quad (4a)$$

$$= \begin{bmatrix} C_{11} & C_{12} & C_{13} & C_{14} & C_{15} & C_{16} \\ & C_{22} & C_{23} & C_{24} & C_{25} & C_{26} \\ & & C_{33} & C_{34} & C_{35} & C_{36} \\ & & & C_{44} & C_{45} & C_{46} \\ & & & & C_{55} & C_{56} \\ & & & & & C_{66} \end{bmatrix}$$

where the lower half of the matrix is implied by symmetry.

Likewise the stress and strain tensors are written in a vector form as follows:

$$\boldsymbol{\sigma} \equiv \begin{bmatrix} \sigma_{xx} \\ \sigma_{yy} \\ \sigma_{zz} \\ \sigma_{yz} \\ \sigma_{xz} \\ \sigma_{xy} \end{bmatrix} \text{ and } \mathbf{e} \equiv \begin{bmatrix} e_{xx} \\ e_{yy} \\ e_{zz} \\ 2e_{yz} \\ 2e_{xz} \\ 2e_{xy} \end{bmatrix}, \quad (4b)$$

after which the stress-strain relationship is written as:

$$\boldsymbol{\sigma} = \mathbf{C}\mathbf{e}. \quad (4c)$$

Note however that (4c) is not a tensor equation – it is not invariant under rotation for example.

### Staggered Fourier derivatives

When a heterogeneous wave equation, such as the elastic wave equation, is used for pseudospectral forward modelling, non-causal ringing artifacts can arise. This phenomenon has been recognized and diagnosed by several authors (Özdenvar and McMechan, 1996; Carcione, 1999). A systematic analysis of the effect is found in (Corrêa et al., 2002), which I summarize here.

Consider a simple 1D scalar wavefield  $u(x)$ . Application of the discrete Fourier domain spatial derivative operator is given by:

$$D_x u = - \sum_{k_x = -k_{Nyq}}^{k_{Nyq}} i k_x \tilde{u}(k_x) \exp(i k_x x), \quad (5)$$

where  $\tilde{u}$  is the discrete Fourier transform of  $u$  taken in the  $x$  direction, and  $k_{Nyq}$  is the Nyquist wavenumber, given by  $k_{Nyq} = \pi/\Delta x$ . The operator applied to  $\tilde{u}$  has the value

$$\pm i k_{Nyq} = \frac{\pi e^{\pm \pi i/2}}{\Delta x},$$

at  $\pm k_{Nyq}$ .

This has two undesirable and physically problematic side effects:

1. The resulting derivative has a pure imaginary Nyquist component, whereas physical (i.e. real valued) wavefields must have real Nyquist.
2. There is a discontinuity in phase (from  $-\pi/2$  to  $\pi/2$ ) at  $\pm k_{Nyq}$ . Recall that in the Fourier domain the wavefield is periodic, with  $-k_{Nyq}$  and  $+k_{Nyq}$  corresponding to the same wavenumber.

It is the second of these effects which is more fundamental. Even if we artificially remove the imaginary Nyquist problem by setting the amplitude at that point to zero, the discontinuity still exists. A discontinuity in the Fourier domain corresponds to a signal in the spatial domain which is non-local (i.e. non-zero everywhere), and so results in ringing artifacts. This problem does not exist for even derivatives, where the operator is equal to  $-k_{Nyq}^2$  for both Nyquist values. This explains why the artifacts arise in the presence of heterogeneities. For a purely homogeneous medium the second derivative operator commutes with the medium properties, so that continuity at Nyquist is restored. However, when there is variation in the medium, the first derivative effects remain present.

Corrêa et al. (2002) show that both of these effects are addressed by adopting a staggered grid, positioned at the half grid points, for computation of the odd derivatives. Why does this correct the problem? Application of the shift operators that move the wavefield forward or backward half a grid point is given by:

$$S_x^\pm u = \sum_{k_g = -k_{Nyq}}^{k_{Nyq}} \exp\left(\mp \frac{ik_x \Delta x}{2}\right) \tilde{u}(k_x) \exp(ik_x x). \quad (6)$$

At the Nyquist wavenumbers,  $\pm k_{Nyq}$ , this operator takes the values  $e^{\mp \pi i/2}$ . Thus when combined with the derivative operator (5) we obtain staggered grid derivative operators:

$$D_x^\pm u = \sum_{k_g = -k_{Nyq}}^{k_{Nyq}} \exp\left(\mp \frac{ik_x \Delta x}{2}\right) ik_x \tilde{u}(k_x) \exp(ik_x x), \quad (7)$$

which have real values at  $\pm k_{Nyq}$ . Moreover there is no longer a phase discontinuity, as the phase is 0 at both  $\pm k_{Nyq}$ .

In order to return the second derivative to the original grid location,  $D_x^+$  is used for the first derivative, whilst  $D_x^-$  is used for the second. To ensure the correct model elastic properties are applied, they must also be interpolated to the intermediate grid positions.

### Staggered grid for 3D anisotropic elastic modelling

When extending this principle to the elastic equation in 3D, there are a couple of additional considerations. Firstly, the staggering is performed along each spatial axis, giving rise to a total of 7 staggered nodes for each node in the original grid. Secondly, computation of the strain tensor involves mixed derivatives, involving differentiation with respect to the 3 spatial coordinates, using operators  $D_x^\pm$ ,  $D_y^\pm$  and  $D_z^\pm$ . The choice of nodes for each computation is determined by the directions of derivatives involved, and becomes somewhat complex.

Carcione (1999) gave a solution to this staggering problem for the 2D VTI case. In fact his solution is general enough to use for orthorhombic symmetries aligned with the computational grid, as it only assumes a Voigt matrix of the following form:

$$C \equiv \begin{bmatrix} C_{11} & C_{12} & C_{13} & & & \\ C_{12} & C_{22} & C_{23} & & & \\ C_{13} & C_{23} & C_{33} & & & \\ & & & C_{44} & & \\ & & & & C_{55} & \\ & & & & & C_{66} \end{bmatrix}, \quad (8)$$

with zeros in the absent positions. The same solution also applies for 3D, where the staggered grid is shown (with a slight abuse of the playing card symbols) in Figure (1). The wavefield derivatives and material property values for each node are given in Table 1, the stress-strain relationships in Table 2 and the equations of motion in Table 3.

The trick that makes this work is that the stresses and strains are defined on the same nodes for all non-zero stiffness coefficients.

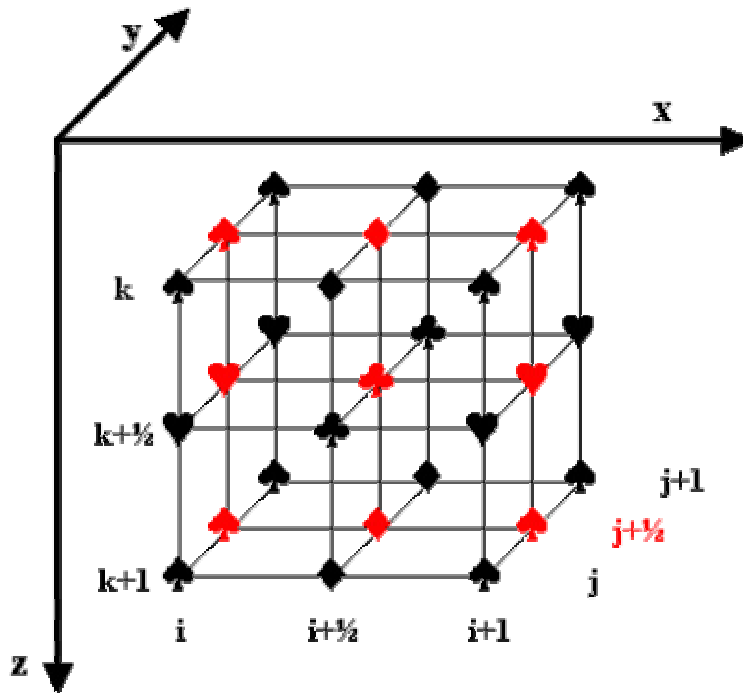


FIG 1. Staggered grid arrangement for 3D modelling of elastic wave propagation.

Table 1. Staggered node properties

Node	Indices	Physical properties
♠	(i, j, k)	$\sigma_{xx}, \sigma_{yy}, \sigma_{zz}, C_{ij}$ (i, j, k ≤ 3) :
♦	(i+1/2, j, k)	$u_x, f_x, \rho$
♠	(i, j+1/2, k)	$u_y, f_y, \rho$
♥	(i, j, k+1/2)	$u_z, f_z, \rho$
♦	(i+1/2, j+1/2, k)	$\sigma_{xy}, C_{66}$
♣	(i+1/2, j, k+1/2)	$\sigma_{xz}, C_{55}$
♥	(i, j+1/2, k+1/2)	$\sigma_{yz}, C_{44}$
♣	(i+1/2, j+1/2, k+1/2)	Unused

Table 2. Stress-strain equations on staggered nodes

Node	Indices	Stress-strain equations
♠	(i, j, k) : (i<4, j<4)	$\sigma_{xx} = C_{11}D_x^-u_x + C_{12}D_y^-u_y + C_{13}D_z^-u_z$ $\sigma_{yy} = C_{21}D_x^-u_x + C_{22}D_y^-u_y + C_{23}D_z^-u_z$ $\sigma_{zz} = C_{31}D_x^-u_x + C_{32}D_y^-u_y + C_{33}D_z^-u_z$
♦	(i+1/2, j+1/2, k)	$\sigma_{xy} = C_{66}(D_y^+u_x + D_x^+u_y)$
♣	(i+1/2, j, k+1/2)	$\sigma_{xz} = C_{55}(D_z^+u_x + D_x^+u_z)$
♥	(i, j+1/2, k+1/2)	$\sigma_{yz} = C_{44}(D_z^+u_y + D_y^+u_z)$

Table 3. Equations of motion on staggered nodes

Node	Indices	Equation of motion
♦	(i+1/2, j, k)	$D_x^+\sigma_{xx} + D_y^-\sigma_{xy} + D_z^-\sigma_{xz} = \rho\ddot{u}_x + f_x$
♠	(i, j+1/2, k)	$D_x^-\sigma_{xz} + D_y^+\sigma_{yy} + D_z^-\sigma_{yz} = \rho\ddot{u}_y + f_y$
♥	(i, j, k+1/2)	$D_x^-\sigma_{xz} + D_y^-\sigma_{yz} + D_z^+\sigma_{zz} = \rho\ddot{u}_z + f_z$

For anisotropy with symmetries of lower order than orthorhombic, or when the axis of anisotropy is not aligned with the grid, this is no longer possible (Igel et al., 1995). In this case we must use shifting operators  $S_x^\pm, S_y^\pm$  and  $S_z^\pm$ , of the form given in equation 6, to relocate strains prior to the multiplication by the stiffness matrix. For example, if  $C_{64} \neq 0$ , then we must map  $e_{yz} = 1/2(u_{y,z} + u_{z,y})$  from node  $(i, j+1/2, k+1/2)$  to node  $(i+1/2, j+1/2, k)$  using  $S_z^-$  followed by  $S_x^+$ , as depicted for the 2D case in Figure 2. I refer to these parts of the stiffness matrix as “non-aligned”.

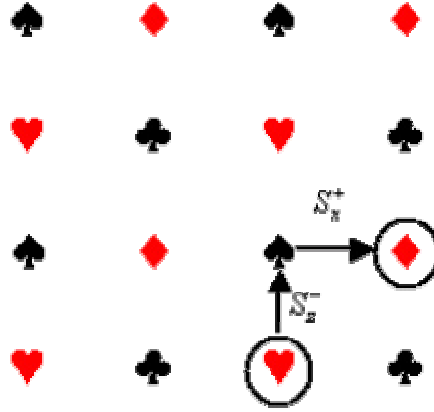


FIG. 2: Shift operations for applying  $C_{64}$  to  $e_{yz}$ . These introduce unavoidable ringing artifacts.

Note that we can choose at which point during this shifting operation to multiply by the stiffness matrix. This flexibility is now exploited to simplify the computation. With an appropriate choice of nodes for the  $C_{ij}$  values, the complete staggered stiffness matrix, including required shift operations can be written as:

$$\mathbf{C}_{stag} = \begin{bmatrix} C_{11} & C_{12} & C_{13} & C_{14} S_y^- S_z^- & C_{15} S_x^- S_z^- & C_{16} S_x^- S_y^- \\ C_{21} & C_{22} & C_{23} & C_{24} S_y^- S_z^- & C_{25} S_x^- S_z^- & C_{26} S_x^- S_y^- \\ C_{31} & C_{32} & C_{33} & C_{34} S_y^- S_z^- & C_{35} S_x^- S_z^- & C_{36} S_x^- S_y^- \\ S_y^+ S_z^+ C_{41} & S_y^+ S_z^+ C_{42} & S_y^+ S_z^+ C_{43} & C_{44} & S_y^+ S_z^+ C_{45} S_x^- S_z^- & S_y^+ S_z^+ C_{46} S_x^- S_y^- \\ S_x^+ S_z^+ C_{51} & S_x^+ S_z^+ C_{52} & S_x^+ S_z^+ C_{53} & S_x^+ S_z^+ C_{54} S_y^- S_z^- & C_{55} & S_x^+ S_z^+ C_{56} S_x^- S_y^- \\ S_x^+ S_y^+ C_{61} & S_x^+ S_y^+ C_{62} & S_x^+ S_y^+ C_{63} & S_x^+ S_y^+ C_{64} S_y^- S_z^- & S_x^+ S_y^+ C_{65} S_x^- S_z^- & C_{66} \end{bmatrix}$$

which can be factorized as follows:

$$\mathbf{C}_{stag} = \mathbf{C}_A + \mathbf{S}^+ \mathbf{C}_B \mathbf{S}^-, \quad (9)$$

where  $\mathbf{S}^\pm = \begin{bmatrix} 1 & & & & & \\ & 1 & & & & \\ & & 1 & & & \\ & & & S_y^\pm S_z^\pm & & \\ & & & & S_x^\pm S_z^\pm & \\ & & & & & S_x^\pm S_y^\pm \end{bmatrix},$

$$\mathbf{C}_A = \begin{bmatrix} C_{11} & C_{12} & C_{13} & & & \\ C_{21} & C_{22} & C_{23} & & & \\ C_{31} & C_{32} & C_{33} & & & \\ & & & C_{44} & & \\ & & & & C_{55} & \\ & & & & & C_{66} \end{bmatrix},$$

and  $\mathbf{C}_B = \begin{bmatrix} & & & C_{14} & C_{15} & C_{16} \\ & & & C_{24} & C_{25} & C_{26} \\ & & & C_{34} & C_{35} & C_{36} \\ C_{41} & C_{42} & C_{43} & 0 & C_{45} & C_{46} \\ C_{51} & C_{52} & C_{53} & C_{54} & 0 & C_{56} \\ C_{61} & C_{62} & C_{63} & C_{64} & C_{65} & 0 \end{bmatrix},$

where again, absent values indicate zeros.

The stress-strain equation is then written in matrix form as follows:

$$\begin{aligned} \boldsymbol{\sigma} &= \mathbf{C}_{stag} \mathbf{e} \\ &= (\mathbf{C}_A + \mathbf{S}^+ \mathbf{C}_B \mathbf{S}^-) \mathbf{e}. \\ &= \boldsymbol{\sigma}_A + \boldsymbol{\sigma}_B \end{aligned} \quad (10)$$

Based on equation (10) the diagonal shift matrices  $\mathbf{S}^\pm$  can now be applied as pre- and post-multipliers to handle the non-aligned terms, as follows:

1. Multiply the strain vector  $\mathbf{e}$  by  $\mathbf{C}_A$  using the staggered grid definitions in Tables 1-3. This gives the “aligned” stress vector  $\boldsymbol{\sigma}_A$ . No shifting operations are required.
2. Pre-multiply the strain vector  $\mathbf{e}$  by  $\mathbf{S}^-$ . This has the effect of mapping all strain grid nodes to (i,j,k), the original grid.
3. Multiply by  $\mathbf{C}_B$  to determine “non-aligned” stresses at these nodes.

4. Post-multiply the stress vector by  $\mathbf{S}^+$  to return them to their staggered nodes. This yields the “non-aligned” stress vector  $\boldsymbol{\sigma}_B$ .
5. Sum  $\boldsymbol{\sigma}_A$  to  $\boldsymbol{\sigma}_B$  to get the total stress.

The need to apply shifting operators is regrettable, as it reintroduces the Nyquist discontinuities (and hence the resulting artifacts) for those terms in the equation, but it appears unavoidable. The scheme described above ensures that those “aligned” stress terms,  $\boldsymbol{\sigma}_A$ , that conform to orthorhombic symmetry are devoid of artifacts, and only the “non-aligned” stresses,  $\boldsymbol{\sigma}_B$  are adversely affected.

### Use of complex FFTs

As remarked in Carcione et al. (2002), it is possible to compute the pseudospectral derivatives of two grid lines simultaneously using complex FFTs. The procedure is to place one function in the real part and one in the imaginary part, feed the result to a complex FFT routine, multiply the result by  $-ik$ , and then inverse FFT the output. The real part and imaginary parts are the derivatives of the two lines. However, this procedure assumes both inputs and *outputs* are real functions, implying hermitian symmetry of their Fourier transforms (in particular a real Nyquist value). Hence this can only strictly be applied in conjunction with staggered grids, such that the odd derivatives are indeed purely real functions. This is true for the aligned case, but not for the non-aligned case (if  $\mathbf{C}_B \neq 0$  above). In the examples below, I simply zero the Nyquist component for this case (e.g. in Figure 7(d)-(f)).

## EXAMPLES

To test the effect of staggering I use a 3D model (Figure 3) consisting of a low-density isotropic cube, enclosed in a higher density medium, which is transversely isotropic with a horizontal symmetry axis (HTI). Modelling is done using a grid of size  $n_x=n_y=n_z=128$  and  $\Delta x=\Delta y=\Delta z=20\text{m}$ . The source is a vertical point force at the center of the grid, with a zero-phase Ricker time signature. Two different anisotropic cases are modeled.

Figure 4 shows the different structures of the stiffness matrix for the outer medium in the two HTI cases. The first (Figure 4a) has an axis of symmetry which is aligned with the grid x direction. The second (Figure 4b) has an axis of symmetry that is at  $45^\circ$  from the x axis. Note that this rotation of the symmetry axis relative to the grid generates further non-zero stiffnesses, which are not “aligned”, and so cannot be staggered exactly.

Figure 6 shows, highly amplified, the early time (100ms) wavefield for the model in Figure 3, with the HTI symmetry axis of the outer medium aligned with the x direction (Figure 4(a)). The geometry of the constant y and constant z slices used are indicated in Figure 3. The plots in the left hand column, (a)-(c), show modelling on a standard (non-staggered) grid. The non-local behaviour of the odd derivative operators interacts with the presence of material property changes at the cube sides, and gives rise to the artifacts in these snapshots. Compare these with the right hand column plots, (d)-(f), where the modelling has been repeated for the same model, but using a staggered grid. Since the

stiffness matrix is “aligned” for this case, the staggered approach does a very good job of suppressing the non-causal artifacts.

In Figure 7, plots (a)-(c) show the result of modelling on a standard grid, for the model in Figure 3, with the HTI symmetry axis of the outer medium at  $45^\circ$  to the x direction (Figure 4(b)). As before we see artifacts arising at the cube sides. Compare these with (d)-(f), where the modelling has been repeated for the same model, but using a staggered grid. The staggered grid modelling reduces most of the artifacts. However, the horizontal slice for the vertical component, (e), displays artifacts which arise from the non-aligned terms in the stiffness matrix. These terms require shifting operations applied to the stress and strain vectors in order to map to them to common grid nodes (see equation (10)), and the shifting operations introduce the artifacts.

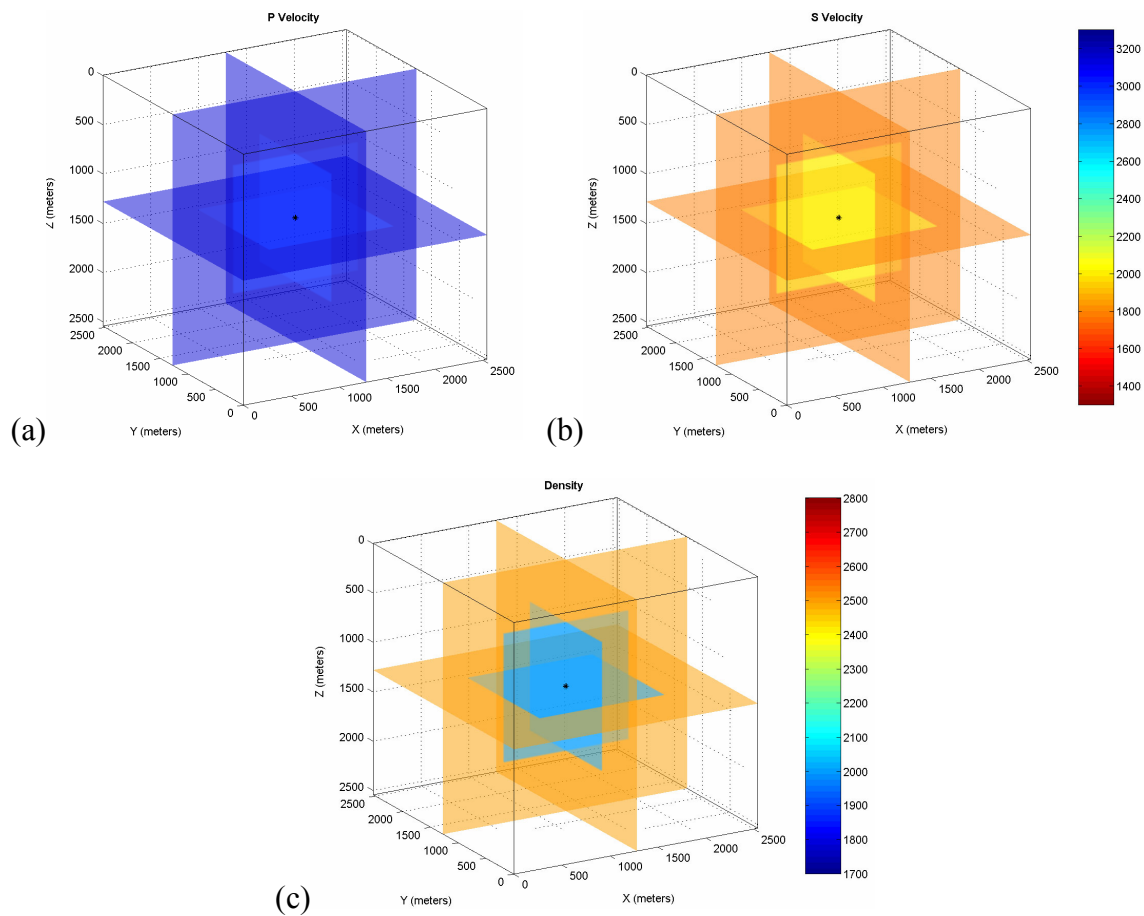


FIG. 3: Elastic properties of 3D model used to test staggered grid modelling. The model consists of an isotropic cube, 1280 meters (64 grid points) on a side, inside an HTI medium. Properties are displayed along three slices, perpendicular to the grid axes, through the source position at the center of the cube. The figures show the fast velocities for  $V_P$  (a) and  $V_S$  (b), in m/s. The velocities inside the cube are  $V_P=3000$  m/s and  $V_S=2000$  m/s. The density (c) is  $2000 \text{ kg/m}^3$  inside the cube, and  $2500 \text{ kg/m}^3$  elsewhere.

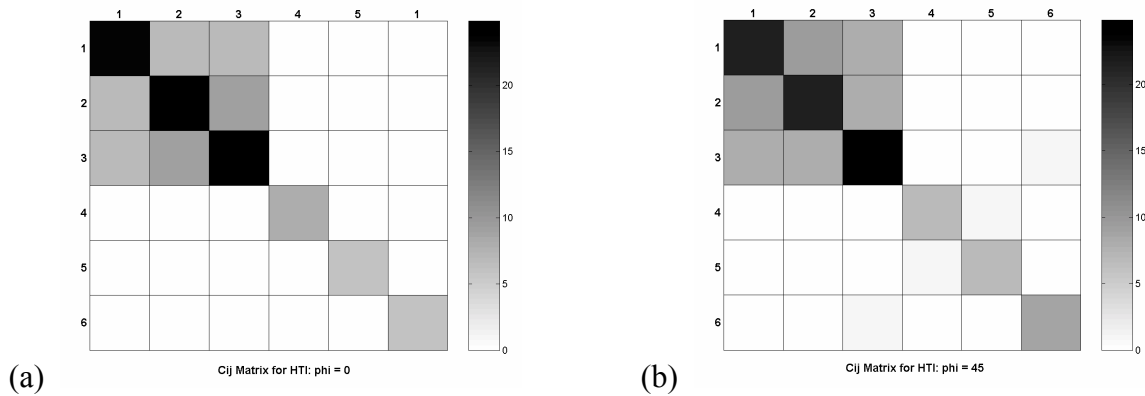


FIG. 4: Stiffness matrices. Each square is grey-scale coded in GPa for the value of the element in that position. For an HTI axis aligned with the x axis, (a), the only non-zero terms are in the upper left quadrant and the lower right diagonal. When the HTI axis is rotated  $45^\circ$  from the x axis, (b), the matrix has further non-zero terms, which cannot be exactly staggered.

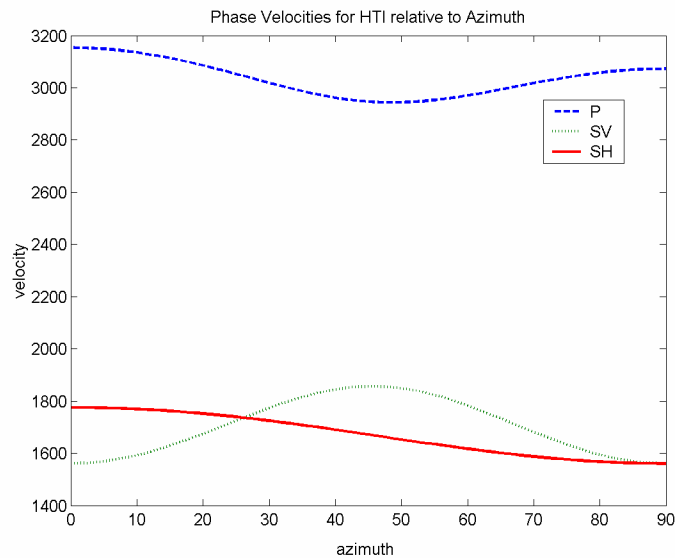


FIG. 5: Phase velocities as a function of azimuth relative to principal axes.

## CONCLUSIONS

The use of staggered grids improves the fidelity of pseudospectral modelling, removing unwanted non-causal artifacts. It does so by forcing the phase spectrum of the odd derivatives to have continuity at the Nyquist wavenumber, resulting in spatially compact operators. Staggered grids may be constructed which achieve this exactly for 3D anisotropic media with orthorhombic or higher symmetries, provided the symmetry planes are aligned with the grid. When this is not the case, then the stiffness matrix may be decomposed into aligned and non-aligned parts, with shift operators used to assist the staggering on the non-aligned part. This results in an imperfect solution, but the artifacts are nonetheless considerably suppressed. These observations are supported by a simple 3D example of an isotropic cube in an anisotropic background.

## ACKNOWLEDGEMENTS

I would like to thank WesternGeco for funding my research as well as other sponsors of the CREWES project for their support.

This work has benefited a great deal from the influence of both Gary Margrave and Ed Krebes, whom I also thank for their careful reviews. In addition, I would like to acknowledge the help, support and advice of several other individuals: Rob Stewart, Kangan Fang, Peter Manning, and Jon Downton; Jim Gaiser, Steve Horne and Johann Robertsson all of WesternGeco; and Jose Carcione of Istituto Nazionale di Oceanografia e di Geofisica Sperimentale.

## REFERENCES

- Carcione, J. M., 1999, Staggered mesh for the anisotropic and viscoelastic wave equation: *Geophysics*, **64**, 1863-1866.
- Carcione, J. M., Herman, G. C. and ten Kroode, A. P. E., 2002, Seismic modelling: *Geophysics* **67**, 1304-1325.
- Cerjan, C., Kosloff, D., Kosloff, R. and Reshef, M., 1985, A nonreflecting boundary condition for discrete acoustic and elastic wave equations: *Geophysics*, **50**, 705-708.
- Collino, F. and Tsogka, C., 2001, Application of the perfectly matched absorbing layer model to the linear elastodynamic problem in anisotropic heterogeneous media: *Geophysics*, **66**, 294-307.
- Corrêa, G. J. P., Spiegelman, M., Carbotte, S., and Mutter, J. C., 2002, Centered and staggered Fourier derivatives and Hilbert transforms: *Geophysics*, **67**, 1558-1563.
- Dablain, M. A., 1986, The application of high-order differencing to the scalar wave equation: *Geophysics*, **51**, 54-66.
- Fornberg, B., 1987, The pseudospectral method - Comparisons with finite differences for the elastic wave equation: *Geophysics*, **52**, 483-501.
- Igel, H., Mora, K., and Riollet, B., 1995, Anisotropic wave propagation through finite-difference grids: *Geophysics*, **60**, 1203-1216.
- Kosloff, D., and Baysal, E., 1982, Forward modelling by a Fourier method: *Geophysics*, **47**, 1402-1412.
- Özdenvar, T. and McMechan, G. A., 1996, Causes and reduction of numerical artifacts in pseudo-spectral wavefield extrapolation: *Geophys. J. Int.*, **126**, 819-828.

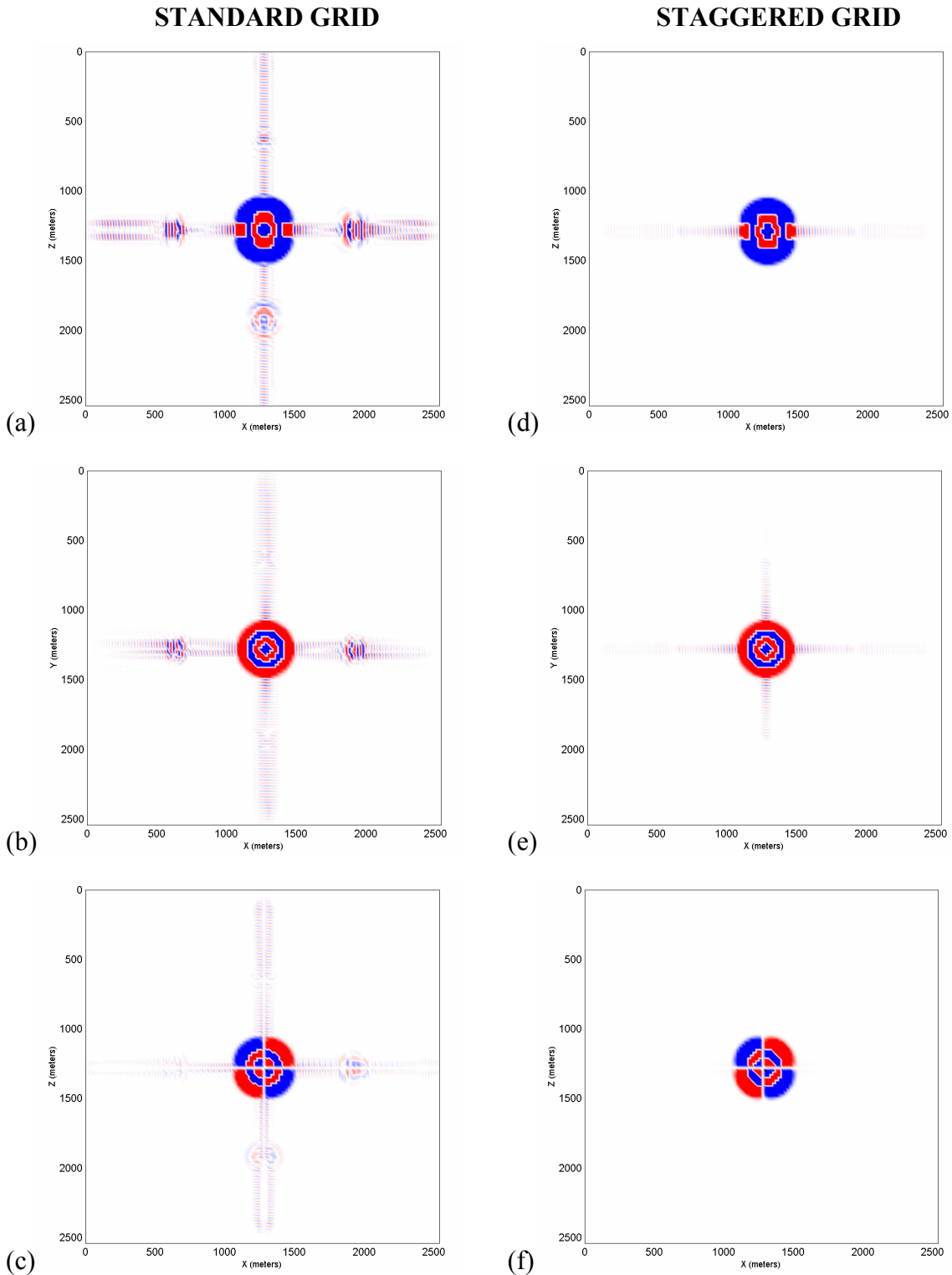


FIG. 6: Standard (a-c) vs. staggered (d-f) grid modelling in model of Figure 3 with HTI symmetry axis along x direction. Snapshots are after 100ms through elastic wavefield along planes of Figure 3. Shown are: (a,d) vertical (Z) component for constant y plane; (b,e) vertical component for constant z plane; (c,f) inline (X) component for constant y plane. Material changes at cube sides reveal non-causal ringing artifacts on standard grid, which are suppressed by staggering.

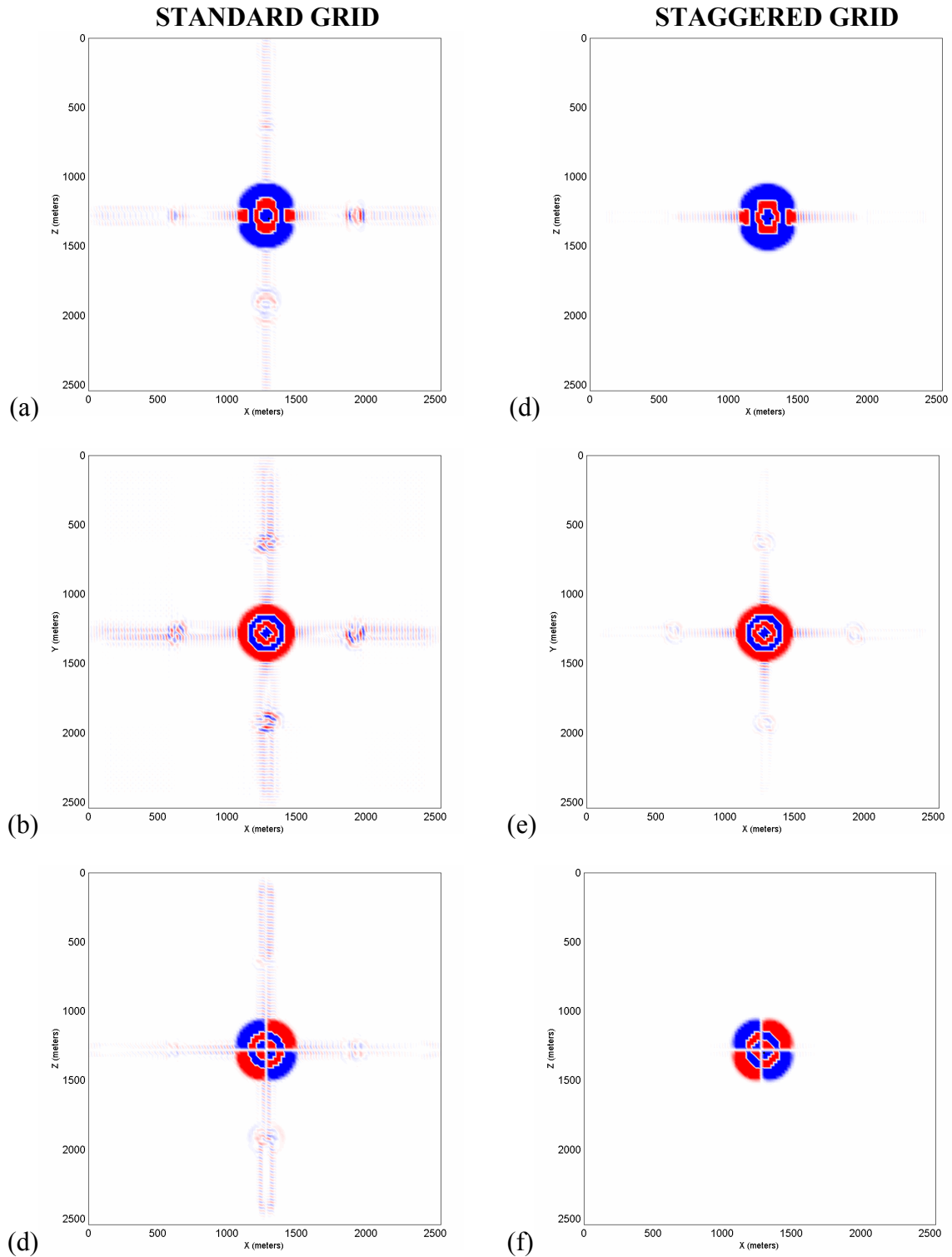


FIG. 7: Standard (a-c) vs. staggered (d-f) grid modelling in model of Figure 3 with HTI symmetry axis at  $45^\circ$  to x direction. Snapshots are after 100ms through elastic wavefield along planes of Figure 3. Shown are: (a, d) vertical (Z) component for constant y plane; (b, e) vertical component for constant z plane; (c, f) inline (X) component for constant y plane. The residual artifacts in (d) and (e) are a result of the non-aligned terms in the stiffness matrix (Figure 4(b)).